

# A miniature electron beam pumped laser

C. Skrobo<sup>1</sup>, T. Heindl<sup>1</sup>, R. Krücken<sup>1</sup>, A. Morozov<sup>1</sup>, R. Steinhübl<sup>1</sup>, J. Wieser<sup>1,2</sup>, and A. Ulrich<sup>1,a</sup>

<sup>1</sup> Physik Department E12, Technische Universität München, James Franck Str. 1, 85748 Garching, Germany

<sup>2</sup> Coherent GmbH, Zielstattstr. 32, 81379 München, Germany

Received 19 February 2009

Published online 16 June 2009 – © EDP Sciences, Società Italiana di Fisica, Springer-Verlag 2009

**Abstract.** The 1.73  $\mu\text{m}$  XeI laser has been operated in a fully continuous mode using a table-top electron beam pumped laser setup. A 12 keV electron beam sent through a 300 nm thick silicon nitride membrane into a laser gas mixture of typically 600 mbar gas pressure was used for pumping. A low loss cavity was installed, resulting in a very low pumping power of 37 mW to reach laser threshold. The geometrical conditions for the laser setup such as the shape of the beam pumped volume and its overlap with the optical mode volume are discussed. The laser scheme has been clearly identified as a recombination laser scheme by operating the laser in pulsed mode and observing the time structure of the laser pulse.

**PACS.** 42.55.Lt Gas lasers including excimer and metal-vapor lasers – 41.75.Fr Electron and positron beams – 42.60.By Design of specific laser systems – 42.60.Pk Continuous operation

## 1 Introduction

A very large number of various gas laser systems is known [1]. The table by Beck et al. from 1980, for example, has 6100 entries [2]. They span a wide wavelength range from roughly 0.110 to 2000  $\mu\text{m}$ . This range is even wider if the more recently developed so called X-ray lasers are also considered as gas lasers. Only a limited number of principle schemes of operation, however, have found their way into practical use: excimer lasers, ion lasers, the nitrogen, helium-neon, and the carbon dioxide lasers for example. Applications range from medical treatment and photolithography with the UV excimer lasers to industrial processes like cutting and welding with the CO<sub>2</sub> laser in the infrared.

There is also only a limited number of pumping methods which can be applied for gas laser operation. Electron collisional excitation is the predominant fundamental process since optical pumping, with the exception of the iodine laser, is normally inefficient for gas lasers. Various forms of gas discharges from intense, short-pulse discharges in dense gases to low power, low pressure dc-discharges are the most widely used way for producing the fast electrons for collisional excitation and ionization of the laser gas species.

Particle beam pumping is an alternative to discharge pumping. The main difference lies in the fact that in a discharge, the electrons are accelerated in the laser medium, whereas they are continuously slowed down when an externally produced particle beam is sent into the laser gas.

Therefore, particle beam pumping avoids run-away effects which limit for example the pumping pulse duration in the case of discharge pumped excimer lasers. The traditional method of particle beam pumping is electron beam pumping [3–5]. Nuclear pumping [6] is a more unusual way for pumping gas lasers. Our group had introduced heavy ion beam pumping into the field in the early 1980s [7,8] and revisited recently with the high intensity ion beams which have now become available [9]. In fission fragment nuclear pumped lasers as well as heavy ion beam pumped lasers the secondary electrons also play an important role in the actual pumping process.

About ten years ago we have developed a way to scale down the devices for electron beam excitation of dense gases to table-top and even portable size. The key innovation for this development was to reduce the thickness of the membrane separating the vacuum in which the electrons are accelerated from the target gas. This became possible by using only 300 nm thick ceramic foils (e.g. silicon nitride) instead of metal foils which require a thickness of several micrometers to be vacuum tight. These thin membranes allow us to use electron energies on the order of 10 keV with tolerable energy and consequently power losses in the entrance foil [10]. The technology and the advantages such as drastically increased power densities which can be produced in the target gas have already been described in the context of incoherent excimer light sources and their applications [11]. In reference [12], we have also already demonstrated the possibility to use the low energy electron beams for gas laser pumping.

Here we describe the technological progress since our first publication [10] which has led us, to our best

<sup>a</sup> e-mail: andreas.ulrich@ph.tum.de

knowledge, to the smallest electron beam pumped gas laser which could be realized, so far. The overall size of the instrument is now only 14 cm in length and 4 cm in diameter compared with roughly 60 cm length and 10 cm diameter in reference [12] (not counting the vacuum pumps and laboratory gas supply systems in both cases). With this instrument the 1.73  $\mu\text{m}$  XeI laser could be pumped fully continuously in a dense argon-xenon mixture. The pumping power to reach laser threshold is now 0.037 W compared with previously 5.3 W. This is a reduction by a factor of about 150. In pulsed mode a wide range of pumping pulse durations and the corresponding time structure of the laser pulse as well as the geometrical shape of the laser beam have been studied.

## 2 Experimental setup

The electron beam pumped laser described here is essentially transversely pumped. However, the laser medium has an almost spherical geometry. A schematic drawing of the setup is shown in Figure 1. The size of the laser setup is demonstrated by the photograph shown in Figure 2. The setup consists of a vacuum cell in which the electron beam is formed and a laser cell with the optical axis perpendicular to the electron beam axis. The two parts are separated by one of the ceramic membranes shown in the inset of Figure 2.

A 12 keV electron beam is formed using an electron gun as it is normally used in monochrome cathode ray tubes. The electron gun was glued into a quartz tube which was pumped with a small turbo molecular pump to a vacuum better than  $10^{-6}$  mbar. A ceramic  $2 \times 2 \text{ mm}^2$  membrane consisting of a 250/50 nm  $\text{Si}_3\text{N}_4/\text{SiO}_2$  layer manufactured on a  $5 \times 5 \text{ mm}^2$  piece of a silicon wafer was glued onto an invar flange. This membrane separated the laser gas from the vacuum in the electron gun part of the setup. Two sets of dipole magnets mounted outside the quartz tube were used to steer the electron beam through the membrane. Focusing of the beam was performed by the electrostatic focusing electrodes of the electron gun. A description of the technique can also be found in references [13,14] in the context of incoherent electron beam pumped light sources.

The electron gun was operated with a regulated and computer controlled power supply (Coherent company). This allowed us to stabilize the dc electron beam current as well as the average current for pulsed operation within approximately 20 nA. Recent experiments have shown that the 12 keV electron energy was stabilized within  $\pm 60$  eV by the power supply [13]. Fully continuous or average electron beam currents from typically 1 to 20  $\mu\text{A}$  were used for both the dc and pulsed experiments. Beam current measurements could be performed via the reading from the power supply and a current pick-off (Rogowski) coil around the cathode lead during pulsed operation, respectively. The electron source was connected to the laser cell via a standard 16 mm vacuum flange (CF16) sealed with a copper gasket.

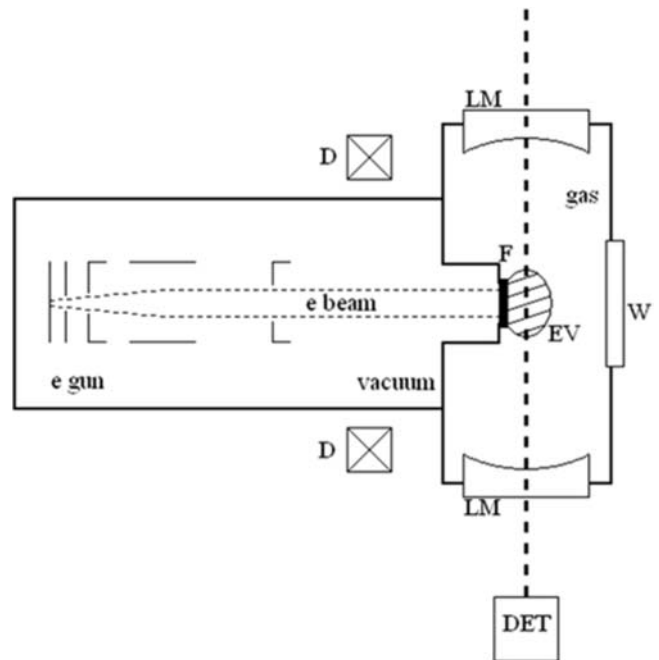


**Fig. 1.** The schematic drawing shows the vacuum part of the electron beam pumped laser on the left side. The electron beam is produced by a hot cathode and extracted and accelerated to 12 keV by a set of grids. An electrostatic lens and two sets of external dipole magnets (D) are used to steer the beam through a thin ceramic foil (F) into the laser gas contained in the right part of the setup. There the electron beam is stopped leading to the electron beam excited volume EV. This is placed between two laser mirrors LM. The optical axis of the resonator is indicated by the dashed line. Laser light is detected with infrared photodiodes (DET). The  $\text{MgF}_2$  window W can be used to observe the light output perpendicular to the laser axis and to perform spectroscopic studies of the spontaneous emission from the laser medium.

A cylindrically shaped laser cell was manufactured from stainless steel with CF16 flanges on both ends and a 10 mm central bore (see Fig. 1). Four additional ports were added to the cell to form a double cross. Two of these ports were used to attach the gas in- and outlet and the other ones were shaped in a way to hold the 12 mm diameter laser mirrors in place. The laser mirrors were also used to seal the gas cell.

The flange holding the membrane used as the entrance window for the electron beam was designed to let the beam enter the laser gas at a distance of 0.6 mm from the laser axis. This design was based on studies concerning the range of the electrons and the shape of beam pumped volume which are discussed in detail in reference [15]. This geometrical design was based on an effective range of the electrons on the order of 1 mm in argon at atmospheric pressure and the typical diameter of the laser beam waist of  $\text{TEM}_{00} = 0.18 \text{ mm}$  for an optimum overlap of the laser beam and the electron beam pumped volume.

Two concave fused silica mirrors with dielectric reflective coating optimized for 1.73  $\mu\text{m}$  (reflectivity of 99.7%) were used to form a low loss optical cavity for

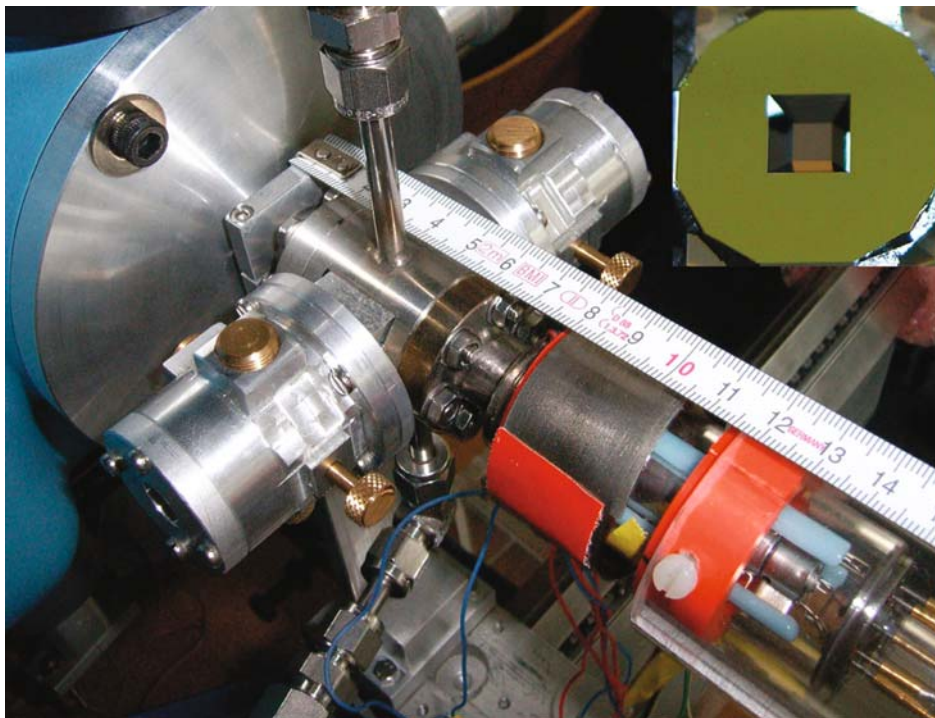


**Fig. 2.** (Color online) Photograph of the electron beam pumped laser. The electron source can be seen in the lower right side of the photograph. The laser cell is the cylindrical volume below the vertical gas inlet line. The optical axis is approximately at the position 4 cm of the tape measure and extends from the lower left to the upper right corner. The two cylindrical housings around the laser axis contain tubes which push the laser mirrors attached to their ends against O-ring gaskets in the laser cell. The adjustment screws visible at these housings push sideways against the tubes holding the laser mirrors for tilting the mirrors. The large flange in the left upper corner is the entrance flange to a  $f = 30$  cm vacuum monochromator (Mc Pherson 218). The inset shows a sample of the ceramic membrane.

the ArXe laser. The mirrors had a radius of curvature of  $r = 500$  mm and a diameter of 12 mm. They were placed at a distance of  $R = 15$  mm and mounted at the tips of two tubes. They sealed the laser cell by pushing onto viton O-rings in the laser cell thus allowing some flexibility for alignment. Two sets of micrometer screws were used to adjust the tilt-angle of the mirrors within  $\pm 2^\circ$ . This design resulted in a stable laser cavity ( $1 - R/r = 0.97$ ) with a nominal beam diameter for the TEM-00 Mode of 0.183 mm. The aspect of multi-mode operation will be discussed below. A  $\text{MgF}_2$  window was installed opposite to the entrance foil of the electron beam allowing spectroscopy of the laser gas from the VUV to infrared spectral region. This window could be replaced by a Faraday cup for beam current measurements.

The argon-xenon laser gas mixtures were prepared from research grade gases with 99.998% purity for both argon and xenon. The gas was mixed and further purified circulating it continuously through a rare gas purifier (Mono-Torr PS4-MT3-R-2, SAES Getters) and the laser cell with a metal bellows compressor. Except for the O-ring seals for the laser mirrors only metal gaskets were used in the gas system. Gas samples could be extracted from the gas system into the vacuum of a quadrupole mass spectrometer (Pfeiffer Vacuum QME 200) via a precision needle valve. The gas sampling system was calibrated using well defined mixing ratios of argon and xenon which were pre-

pared under static conditions using a precision capacitive manometer (Baratron 390HA) and sampled under operating conditions for various mixing ratios and pressures.

Laser output was measured with two InGaAs photodiodes (OEC GAP2000/2.2 and Judson 12-LD2-R250U, respectively). They were sensitive in a spectral range from 0.8 to 2.2  $\mu\text{m}$ . The first detector had a diameter of 2 mm. It was partly used behind an aperture of 1 mm diameter to obtain better spatial resolution for laser beam shape measurements. Using pulsed light from an LED it was tested that both detectors had a time resolution better than 1  $\mu\text{s}$ . The photocurrent was measured with a high precision electrometer (Keithley 614) for dc measurements and a fast storage oscilloscope (LeCroy wave Runner 6050) was used for time resolved measurements either with the photodiodes operated on resistors of 50 and 470  $\Omega$ , respectively. The sensitivity of the OEC detector at 1.73  $\mu\text{m}$  was 0.9 A/W.

### 3 Experimental results

#### 3.1 Fully continuous operation of the 1.73 $\mu\text{m}$ ArXe laser

The 1.73  $\mu\text{m}$  ArXe laser has been studied with various pumping methods using both discharge and particle beam

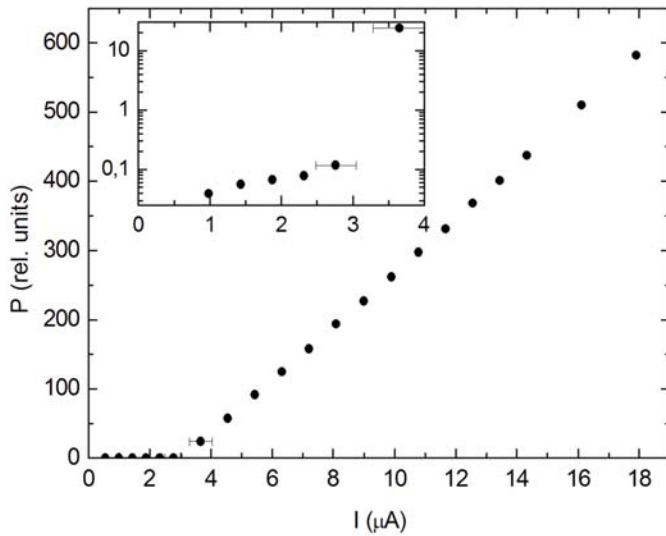


**Fig. 3.** The onset of laser operation is demonstrated by the light output  $P$  plotted versus the electron beam current  $I$ . The inset shows an expanded region around threshold with the intensity shown on a logarithmic scale. The slight increase of spontaneous emission below threshold and the onset of laser operation are clearly visible. The error in the output power is smaller than the size of the data points shown.

excitation [5,16]. With particle beam pumping, electron beams and so called nuclear pumping was applied where fission fragments or the products of a  ${}^3\text{He}(n, p)T$  reaction deposit their energy in the laser medium. In these cases reported in the literature it is not so clear whether or not the ArXe laser could be operated fully continuously or if contamination of the laser gas, temperature rise of the gas, or even some principle aspects of the pumping scheme might limit the maximum duration of a laser pulse. Therefore one of the first goals of the experiments described here was to test if the laser could be operated in the miniature electron beam setup described above, at all, and if so, if a fully continuous operation could be achieved.

For this test the laser cavity was carefully pre-aligned with a HeNe laser and the InGaAs infrared detector was placed on the optical axis. Prior to the test for fully continuous operation the laser was operated in a pulsed mode with parameters similar to the ones used in reference [12] (10  $\mu\text{s}$  pulses, 0.15 mA beam current during the pulses). Laser effect could be obtained with the novel setup easily showing that the laser could also be operated with the miniaturized geometry. This mode of operation was then used to optimize the mirror alignment as well as the laser gas composition.

The optimized mixture of 630 mbar Ar containing 0.5% Xe was filled into the laser cell and the electron beam switched to fully continuous operation. Light output was recorded with increasing (dc) beam current of the electron source. Data are shown in Figure 3. Fully continuous laser operation was achieved above a threshold of 3.1  $\mu\text{A}$ . The inset of Figure 3 shows an expanded view of the data in the region of laser threshold with a logarithmic intensity scale for light output. The steep increase of light output be-

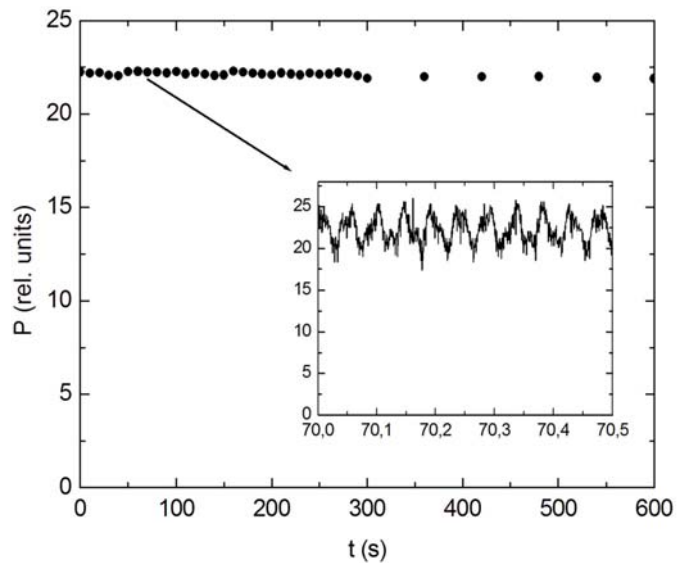


**Fig. 4.** The stability of the laser output of the fully continuously operating 1.73  $\mu\text{m}$  laser is shown for a 10 min time period. The inset shows the stability for a 500 ms time interval.

tween 2.8 and 3.6  $\mu\text{A}$  electron beam current clearly shows the onset of laser operation. Extrapolation of the data in the main graph (linear scale) result in a threshold electron beam current of 3.1  $\mu\text{A}$  which corresponds to a threshold pumping power of only 37.2 mW.

The laser output was monitored over a longer time of 600 s (10 min) to test whether the fully continuous laser output can be maintained without degradation. The data are shown in Figure 4. They show that the 1.73  $\mu\text{m}$  laser can be realized as a near infrared dc-laser with the setup described here.

### 3.2 Mode volume and beam pumped volume

One of the most characteristic features of the miniature electron beam pumped laser described here is the very small, almost spherical beam pumped volume. Therefore it was interesting to study the mode volume of the laser in comparison with the size and shape of the beam pumped volume. The mode volume was derived by observing the laser output and numerical simulation was used to determine the spatial distribution of power deposition in the laser medium.

The size and shape of the beam pumped volume was determined using the model program CASINO [17]. The method and a study of its validity based on the spatial distribution of the emissivity of neon and nitrogen used as the target gas has been published in reference [15]. Here we were interested in the spatial distribution of beam power deposited in the laser medium projected into a plane perpendicular to the direction of the laser beam. This value should be directly correlated with the optical gain which the various sections of the laser beam experience when they pass through the laser medium. Data visualizing this distribution are shown in Figure 5. For calculating

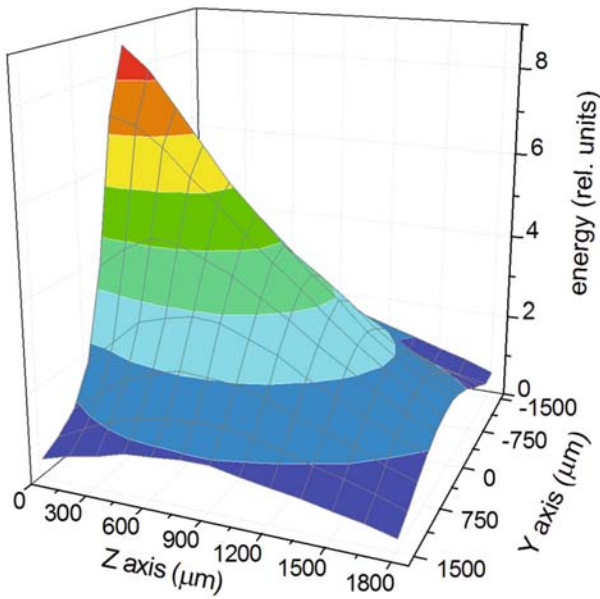


**Fig. 5.** (Color online) The spatial distribution of pumping power density is shown as derived from a model calculation using the program “CASINO”. The  $z$ -axis represents the direction of the electron beam and the  $y$ -axis is perpendicular to the electron- and laser beam direction (see text).

these data the beam excited volume was divided into  $51 \times 51 \times 50$  boxes. The  $z$ -axis represents the (horizontal) electron beam axis. The  $y$ -axis is the vertical direction perpendicular to the electron beam and the optical axis. The power deposition is summed over the  $x$ -direction (= laser axis) and shown on the vertical axis of the plot (Fig. 5). The figure can be interpreted as the pumping power density integrated along the direction of the laser beam for various distances from the entrance foil for the electron beam.

Two independent measurements of the laser beam profile were performed. In one case the (OEC) InGaAs infrared detector was used with the aperture of 1 mm diameter in front and moved up and down and left and right with a  $y$ - $z$  support. Beam profiles were measured at various  $x$ -positions along the laser beam axis for continuous operation of the laser. Examples of the data for the vertical direction are shown in Figure 6. The full beam width calculated at 36.9% ( $1/e$ ) of the peak maximum is shown versus the distance of the center of the laser cavity in Figure 7. A beam diameter of 1.44 mm in the center of the laser cavity can be extrapolated from these data. A comparison with the 0.18 mm which can be calculated for the TEM<sub>00</sub> mode clearly shows the multi-mode character of the laser beam.

As an alternative to measuring the beam profile point by point with the IR detector, an IR-beam profile monitor (Thorlabs model BP 109-IR) was used to observe beam profiles online for various positions along the laser axis and for different laser mirror alignments. This is of interest since the almost spherical gain volume allows the laser axis to be oriented rather freely. Only the membrane

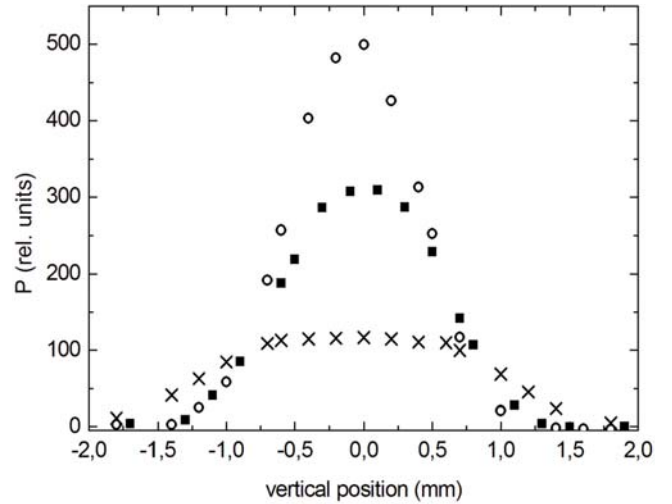


**Fig. 6.** Examples of beam profile measurements are shown for three positions along the laser axis, 11.9 cm (X), 4.9 cm (full squares), and 2.5 cm (open circles) from the center of the optical cavity.

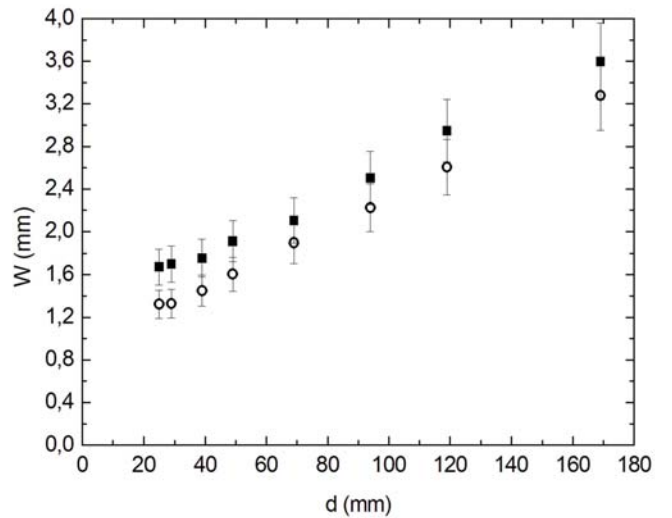


**Fig. 7.** The horizontal (full squares) and vertical (open circles) laser beam width is plotted versus the distance from the center of the laser cavity. A beam diameter of 1.44 mm in the center can be extrapolated from this set of data.

through which the electron beam enters the laser gas and its holder introduce an asymmetry which is visible in the beam profile example shown in Figure 8.

A combination of the beam profile measurements for the optimum alignment of the mirrors and the modelling of the spatial distribution of pumping power in the gas led to the conclusion that for the optimum gas pressure of 630 mbar a fraction of 26.5% of the electron beam power was deposited within the mode volume of the laser beam. Note, that we have used the term “mode volume” in a very general way without specifying the modes which are active in the obviously multi mode laser. Using the total light output which was measured using the signal from the intensity calibrated beam profile monitor to record all

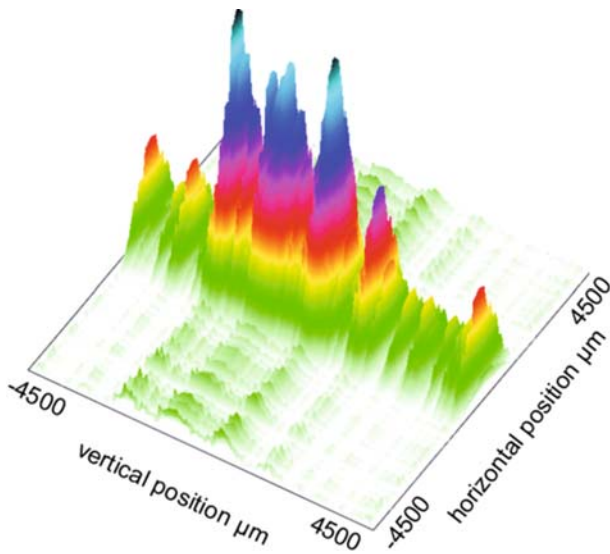


**Fig. 8.** (Color online) An example of a beam profile is shown for a strongly dealigned laser cavity. It shows that many off-axis modes can be made to “lase” due to the almost spherical gain medium.

the light in the beam for optimum mirror alignment we found 0.5 mW laser light for 15  $\mu\text{A}$  electron beam current (0.18 W pumping power). This corresponds to an overall efficiency of 0.28% and about 1% when the laser output power is normalized to the power deposited in the mode volume of the laser. Note that the mirror reflectivity was not optimized for laser output power in the experiments described here.

### 3.3 Time structure of pulsed laser output

Besides the fully continuous operation described above the laser could be pumped with pulsed electron beams within a wide parameter range. Because of the high repetition rate and the wide range of pulse durations which can be applied for pumping, the laser setup is ideally suited for testing the gas kinetics and other effects of the laser gas composition. Here we describe an experiment which shows that the laser is clearly a recombination laser. Based on this observation the influence of helium gas as an additive to the ArXe mixture was tested with the aim to foster the recombination process.

In pulsed mode and for short pulses (less than about one microsecond) the main limitation of the pumping power is given by the specific heat of the membrane since the beam energy deposited in the membrane cannot be cooled off rapidly enough. Therefore the heat capacity of the membrane has to keep it from melting or mechanical softening which starts at about 1000 K. In essence this leads to a beam current-pulse duration product on the order of  $10^{-7}$  As for 12 keV electrons and the present setup with its  $2 \times 2 \text{ mm}^2$  membrane. The power supply used here allowed a minimum pulse duration of 400 ns. Therefore, the maximum beam current was limited here by the maximum current of about 1 mA, which could be provided by

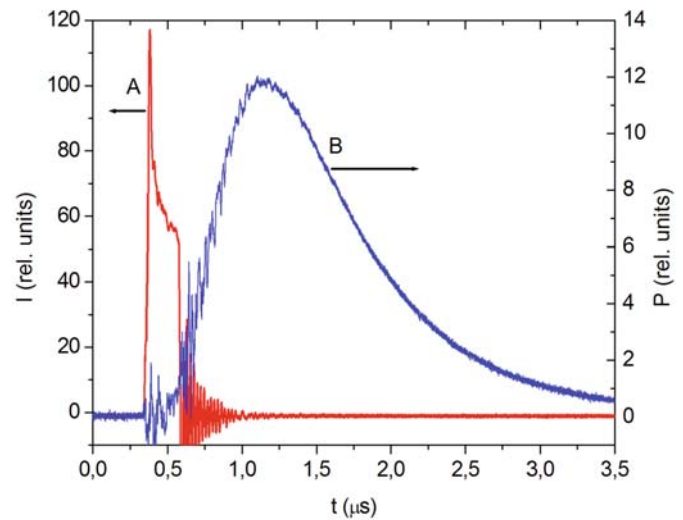


**Fig. 9.** (Color online) The time dependence of the pumping power and the laser output are shown for a 400 ns long pumping pulse. Trace A shows the electron beam current (left scale) and trace B (right scale) the laser output. The data show that the pumping scheme is dominated by recombination processes.

the electron gun rather than the stability of the entrance foil which would have survived the thermal load of 400 ns, 200 mA beam pulses.

An electron beam pulse (max. peak current available ( $\sim 1 \text{ mA}$ ), 400 ns, trace A in Fig. 9) and the corresponding laser pulse (trace B in Fig. 9) show that the laser pulse starts essentially when the 400 ns electron beam pulse has ended and extends over a much longer time, even longer than the  $3.5 \mu\text{s}$  shown in Figure 9. Compared with the fully dc operation this is the other extreme mode of operation of the present setup. The data shown in Figure 9 can be qualitatively interpreted as follows. Assuming the well-known aspect that recombination plays a major role in the pumping process of the ArXe laser [18,19] the low intensity of the laser light during the pulse and its increase after the pulse are an indication that the electron beam produces relatively hot electrons which cool by collisions with the laser gas atoms roughly within  $1 \mu\text{s}$ . At that time after the pulse the electron density is still high but the electron temperature low enough to lead to a high recombination rate. This results in the peak of the laser output. In the later phase the electron density decreases further and the laser output is reduced until it falls below threshold.

The setup described here will be used for more detailed gas kinetic studies of laser media in forthcoming experiments. A favourable influence of helium for the gas kinetics e.g. in the form of improved electron cooling has been discussed in the literature [19]. A brief test of the effect of helium added to a 650 mbar Ar, 3.25 mbar Xe laser gas mixture is shown in Figure 10. The increasing helium concentration leads to two effects. The onset and the decay time of the  $10 \mu\text{s}$  laser pulses reduced from  $1.15 \mu\text{s}$  for pure ArXe to  $0.5 \mu\text{s}$  (10 to 90% values) by adding 500 mbar He. The “overshoot” at the beginning of the laser pulses in Figure 10 can tentatively be attributed to

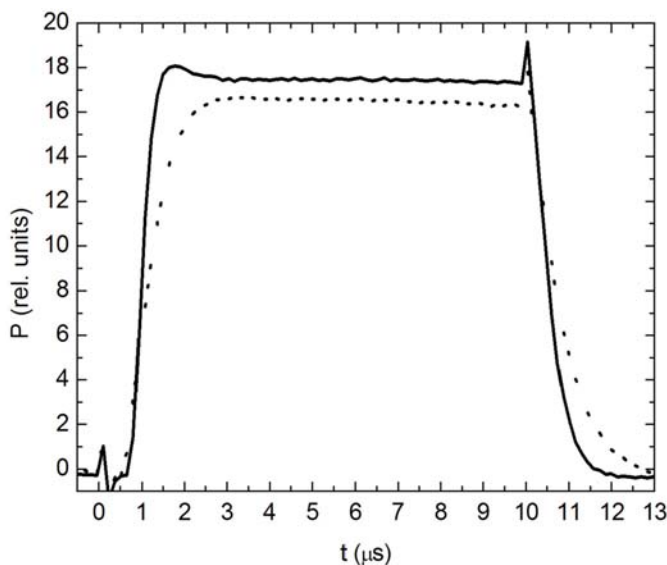


**Fig. 10.** The effect of adding helium to the laser gas on the time dependence of a nominally 10  $\mu\text{s}$  long laser pulse is shown. The dashed trace corresponds to a laser gas of 650 mbar Ar and 3.25 mbar Xe as a reference and the solid line shows the laser output with 500 mbar helium added.

an instrumental effect, namely an overshoot in the electron beam current similar to the one which can be seen for the short pulse in Figure 9. The decay times (measured also for a 90 to 10% intensity change) vary from 1.53  $\mu\text{s}$  to 1.35  $\mu\text{s}$ . The second effect is a slight increase of laser power on the order of 5% during the pulses.

## 4 Summary and outlook

Extremely thin ceramic membranes used as entrance foils for the beam allow the development of miniaturized, table top electron beam pumped lasers. Ongoing technical developments in the context of incoherent ultraviolet light sources [20,21] will allow portable versions in which the vacuum part of the setup is sealed off as in a regular vacuum tube. The large beam current – pulse duration product which is possible for the membranes will be used to pump shorter wavelength lasers in future experiments. This could by far not be reached in the experiments reported here due to the limited beam current provided by the electron gun. Electron guns with again 12 keV electron energy but 2 A beam current (for example: Heat Wave Labs No. 101079) will be used for that purpose.

This work has been funded by the Maier Leibnitz Laboratory Munich. The authors thank the Thorlabs company for lending out the beam profile monitor for infrared wavelengths.

## References

1. *CRC Handbook of Laser Science and Technology, Volume II: Gas Lasers*, edited by M.J. Weber (CRC Press Inc., Boca Raton, FL, USA, 1982)
2. R. Beck, W. Englisch, K. Gürs, *Table of Laser Lines in Gases and Vapors* (Springer, Berlin, Heidelberg, New York, 1980)
3. N.G. Basov, O.V. Bogdankevitch, V.A. Danilychev, A.E. Devyatkov, G.N. Kashnikov, N.B. Lantsov, *JETP Lett.* **7**, 317 (1968)
4. P.W. Hoff, J.C. Swingle, C.K. Rhodes, *Opt. Commun.* **8**, 128 (1973)
5. J.P. Apruzese, J.L. Giuliani, M.F. Wolford, J.D. Sethian, G.M. Petrov, D.D. Hinshelwood, M.C. Myers, D.M. Ponce, F. Hegeler, T. Petrova, *Appl. Phys. Lett.* **88**, 121120 (2006)
6. *Abstracts IV Int. Conf. Physics of Nuclear-Pumped Lasers and Pulsed Nuclear Reactors (NPL-PNR-2007)*, edited by P.P. Dyachenko (Institute of Physics and Power Engineering (IPPE) Obninsk, Russia, 2007)
7. A. Ulrich, H. Bohn, P. Kienle, G.J. Perlow, *Appl. Phys. Lett.* **42**, 782 (1983)
8. A. Ulrich, H.J. Körner, W. Krötz, G. Ribitzki, D.E. Murnick, E. Matthias, P. Kienle, D.H.H. Hoffmann, *J. Appl. Phys.* **62**, 357 (1987)
9. A. Ulrich, A. Adonin, J. Jacoby, V. Turtikov, D. Fernengel, A. Fertmann, A. Golubev, D.H.H. Hoffmann, A. Hug, R. Krücken, M. Kulish, J. Menzel, A. Morozov, P. Ni, D.N. Nikolaev, N.S. Shilikin, V.Ya. Ternovoi, S. Udrea, D. Varentsov, J. Wieser, *Phys. Rev. Lett.* **97**, 153901 (2006)
10. J. Wieser, D.E. Murnick, A. Ulrich, H.A. Huggins, A. Liddle, W.L. Brown, *Rev. Sci. Instrum.* **68**, 1360 (1997)
11. A. Ulrich, J. Wieser, M. Salvermoser und D. Murnick, *Physikalische Blätter* **56**, 49 (2000)
12. A. Ulrich, C. Nießl, J. Wieser, H. Tomizawa, D.E. Murnick, M. Salvermoser, *J. Appl. Phys.* **86**, 3525 (1999)
13. A. Morozov, T. Heindl, C. Skrobol, J. Wieser, R. Krücken, A. Ulrich, *Eur. Phys. J. D* **48**, 383 (2008)
14. A. Morozov, R. Krücken, J. Wieser, A. Ulrich, *Eur. Phys. J. D* **33**, 207 (2005)
15. A. Morozov, R. Krücken, A. Ulrich, J. Wieser, *J. Appl. Phys.* **100**, 093305 (2006)
16. S.N. Tskhai, Yu.B. Udalov, P.J.M. Peters, W.J. Witteman, V.N. Ochkin, *Appl. Phys. B* **62**, 11 (1996)
17. P. Hovington, D. Drouin, R. Gauvin, *Scanning* **19**, 1 (1997) and CASINO v2.42 <http://www.gel.usherbrooke.ca/casino/index.html>
18. M. Ohawa, T.J. Moratz, M.J. Kushner, *J. Appl. Phys.* **66**, 5131 (1989)
19. W.J. Alford, G.N. Hays, M. Ohwa, M.J. Kushner, *J. Appl. Phys.* **69**, 1843 (1991)
20. R. Steinhübl, K. Besenthal, N. Koch, G. Kornfeld, *IEEE Trans. Electron Devices* **52**, 884 (2005)
21. A. Morozov, T. Heindl, R. Krücken, A. Ulrich, J. Wieser, *J. Appl. Phys.* **103**, 103301 (2008)